sustainability

MDPI

Article

Nitrogen Migration during Pyrolysis of Raw and Acid Leached Maize Straw

Huan Li [1,2,3], Huawei Mou [1,2,3], Nan Zhao [1,2,3], Yaohong Yu [1,2,3], Quan Hong [1,2,3], Mperejekumana Philbert [1,2,3], Yuguang Zhou [1,2,3,4,*], Hossein Beidaghy Dizaji [5,*] and Renjie Dong [1,2,3,6]

1 Bioenergy and Environment Science & Technology Laboratory, College of Engineering, China Agricultural University, Beijing 100083, China; huanli828@cau.edu.cn (H.L.); mouhuawei@163.com (H.M.); nan.zhaoca@outlook.com (N.Z.); syyh0613@163.com (Y.Y.); hong_quan97@163.com (Q.H.); philbertson2@yahoo.com (M.P.); rjdong@cau.edu.cn (R.D.)
2 Key Laboratory of Clean Production and Utilization of Renewable Energy, Ministry of Agriculture and Rural Affairs, Beijing 100083, China
3 National Center for International Research of BioEnergy Science and Technology, Ministry of Science and Technology, Beijing 100083, China
4 Prataculture Machinery and Equipment Research Center, College of Engineering, China Agricultural University, Beijing 100083, China
5 Thermo-chemical Conversion Department, DBFZ Deutsches Biomasseforschungszentrum Gemeinnützige GmbH, Torgauer Straße 116, 04347 Leipzig, Germany
6 Yantai Institute, China Agricultural University, No. 2006 Binhai Zhonglu, Laishan District, Yantai 264670, China
* Correspondence: zhouyg@cau.edu.cn (Y.Z.); hossein.beidaghy@dbfz.de (H.B.D.); Tel.: +86-10-62737885 (Y.Z.)

Abstract: Solid biofuel is considered as a possible substitute for coal in household heat production because of the available and sustainable raw materials, while NO_x emissions from its combustion have become a serious problem. Nitrogen-containing compounds in pyrolysis products have important effects on the conversion of fuel-N into NO_x-N. Understanding these converting pathways is important for the environmentally friendly use of biomass fuels. The nitrogen migration during pyrolysis of raw and acid leached maize straw at various temperatures was investigated in this study. Thermal gravimetric analysis and X-ray photoelectron spectroscopy were used to investigate the performances of thermal decomposition and pyrolysis products from samples. The main nitrogen functional groups in biomass and biochar products were N-A (amine-N/amide-N/protein-N), pyridine-N, and pyrrole-N, according to the findings. The most common gaseous NO_x precursor was NH_3, which was produced primarily during the conversion of N-A to pyridine-N and pyrrole-N. The formation of HCN mainly came from the secondary decomposition of heterocyclic-N at high temperatures. Before the pyrolysis temperature increased to 650 °C, more than half of the fuel-N was stored in the biochar. At the same pyrolysis temperature, acid-leached maize straw yielded more gas-N and char-N than the raw biomass. The highest char-N yield of 76.39 wt% was obtained from acid-leached maize straw (AMS) pyrolysis at 350 °C. Low pyrolysis temperature and acid-leaching treatment can help to decrease nitrogen release from stable char structure, providing support for reducing nitrogenous pollutant emissions from straw fuel.

Keywords: maize straw; acid leaching; ash; pyrolysis; nitrogen conversion

check for updates

Citation: Li, H.; Mou, H.; Zhao, N.; Yu, Y.; Hong, Q.; Philbert, M.; Zhou, Y.; Dizaji, H.B.; Dong, R. Nitrogen Migration during Pyrolysis of Raw and Acid Leached Maize Straw. *Sustainability* **2021**, *13*, 3786. https://doi.org/10.3390/su13073786

Academic Editor: Attila Bai

Received: 8 February 2021
Accepted: 23 March 2021
Published: 29 March 2021

Publisher's Note: MDPI stays neutral with regard to jurisdictional claims in published maps and institutional affiliations.

Copyright: © 2021 by the authors. Licensee MDPI, Basel, Switzerland. This article is an open access article distributed under the terms and conditions of the Creative Commons Attribution (CC BY) license (https://creativecommons.org/licenses/by/4.0/).

1. Introduction

Biomass energy is a form of renewable energy derived directly or indirectly from plant photosynthesis. Solid biomass fuel has been gaining popularity as a way to reduce reliance on fossil fuels while also dealing with climate change [1]. However, biomass fuel combustion is reported to result in high NO_x (NO, NO_2, N_2O, etc.) emissions [2]. The NO_x produced from fuel combustion can be divided into thermal-NO_x, fuel-NO_x, and prompt-NO_x according to their origins. The formation mechanism of prompt-NO_x is

complicated and its amount is relatively small. Thermal-NO_x is primarily formed by the reaction of nitrogen and oxygen at high temperatures (>1300 °C) [3]. While the furnace temperature of household biomass stove is mostly lower than 700 °C (refer to previous studies [4,5]), fuel-NO_x accounted for most of all NO_x [6,7]. Fuel-N can be converted into various nitrogen-containing functional groups during the pyrolysis process, and these compounds can react with oxygen to produce various NO_x species [8]. For NO_x regulation, it is critical to have a thorough understanding of the transformation and migration behavior of fuel-N during biomass pyrolysis.

Both biomass characteristics (species, contents of nitrogen, volatile matter and ash content, etc.) and pyrolysis operation conditions (temperature, heating rate, air supply, etc.) influence the pyrolysis performance of the biomass. Researchers investigated the migration course of nitrogen elements in raw biomass, proteins, and N-containing compounds (formed by protein mixed with hemicellulose, cellulose, and lignin) under various operating conditions [9–11]. With the increase of temperature, NO_x precursors are primarily formed by the following three ways: the pyrolysis of unstable fuel-N, secondary decomposition of char, and tar products [12]. The main NO_x gaseous precursors are NH_3, HCN, and HNCO, with HNCO accounting for little and being easily transferred to the other two [13,14]. The dominant N-species are determined by the biomass type and origin. In some biomass, such as sewage sludge, nitrogen mainly exists in the form of heterocyclic-N, HCN can be found to be the main NO_x precursor during pyrolysis [8]. However, the majority of nitrogen in plant residues is found in proteins and free amino acids, with only a small amount in the form of nucleic acid, chlorophyll, enzymes, vitamins, alkaloids, and inorganic nitrogen [15], NH_3 will become the dominant nitrogen-containing precursor [16].

Agricultural and woody residues are the two main materials of solid biofuels. According to the literature, agricultural residues (straw fuels) may have 5–20 times higher ash content than those of woody biomass, which could contribute to inefficient combustion [17]. Besides, alkali and alkaline earth metallic species (AAEMs) in ash (K, Ca, Na, Mg, etc.) are thought to influence the devolatilization and combustion process [18,19]. Acid-leaching treatment can reduce the content of ash and AAEMs, effectively improve the combustion performance and reduce ash melting, slagging, and corrosion [20–23], but the impact of AAEMs on the NO_x precursor generations of biomass pyrolysis remains unclear. Deep research on the effects of de-ashing and demineralization by acid-leaching on nitrogen transfer and conversion would help the clean utilization of straw biomass fuel.

Therefore, nitrogen migration behaviors during pyrolysis of raw and acid-leached maize straw were investigated in this report. To reduce the ash and AAEMs contents in maize straw, pre-treatment of acid-leaching with CH_3COOH was introduced. The thermal gravimetric analysis (TGA) and pyrolysis experiments at various temperatures were performed to evaluate the decomposition characteristics of the two biomass samples. X-ray photoelectron spectroscopy (XPS) was used to investigate the distribution and migration of nitrogen functional groups in biomass and corresponding biochar, and the effect of acid-leaching on NO_x precursors generation was further analyzed.

2. Materials and Methods

2.1. Materials and Pretreatment Process

In this study, raw maize straw (RMS) was obtained from Shangzhuang experimental station of China Agricultural University, Beijing, China. The samples were crushed and sieved through a 100 mesh sieve, then dried in an oven at 105 °C for 12 h.

Various organic and inorganic acids have been used for acid treatment in previous researches. Strong acids, such as sulfuric acid and nitric acid were reported to enhance dehydration reactions in biomass. Hydrochloric acid is also a commonly leaching solution, but chloride ions will affect the subsequent HCN concentration measurement. To effectively remove AAEMs, while reducing the damage to the biomass structure and not introducing other ions [24], CH_3COOH solution was adopted in this study. The solution was prepared by adding 30 mL of glacial acetic acid (1.05 g/mL, 99.5%) into 970 mL of distilled water

and mix thoroughly, which was converted to a mass concentration of 3.13%. Acid-leached maize straw (AMS) was pretreated by soaking 10 g of raw maize straw samples in 200 mL acid solution for 2 h at room temperature while stirring. After removing the acid liquor, the acid-leached biomass was washed with deionized water to neutral pH and then dried at 105 °C for 12 h.

Ultimate analysis of the samples was performed by Vario EL cube (Elementar, Langenselbold, Germany), and oxygen content was detected by difference (Table 1). Proximate analysis of the biomass fuels was carried following the existing Chinese standards [25,26]. The ash content for the biomass sample was reduced from 12.69 wt% to 8.67 wt% after acid treatment. The main residual material in the ash should be silica, since more than half of the ash of the maize straw consists of SiO_2 [27], and it is hardly removed by acid leaching. The contents of cellulose, hemicellulose, and lignin in biomass were determined using the methods mentioned by Guo et al. [28]. To better understand the effect of the pre-treatment, inductively coupled plasma with optical emission spectroscopy (ICP-OES) (ICPOES730, Agilent, Santa Clara, CA, USA) was performed on RMS and AMS to provide selected elemental compositions of the fuel ashes (Table 1). It should be noted that the acid leaching significantly decreased the content of K, Na, and Mg, which were abundantly found in biomass ash.

Table 1. Basic characteristics of the two biomass samples.

Characteristic		Biomass Sample		Removal Ratio %
		RMS	AMS	
Ultimate analysis wt%, dry basis	C	41.83	44.69	
	H	5.08	6.18	
	S	0.58	0.68	
	N	1.39	1.13	
	O [1]	51.13	47.33	
Proximate analysis wt%, dry basis	Volatile matter	68.68	75.70	
	Fixed carbon	16.94	13.01	
	Ash	12.69	8.67	
Composition%	Hemicellulose	31.11	36.49	
	Cellulose	29.03	34.47	
	Lignin	3.72	3.62	
Inorganic elements [2] mg/kg	K	21,245.4	92.1	99.57
	Na	1474.9	61.5	95.83
	Mg	2171.9	91.7	95.78
	P	2254.1	364.4	83.84
	Fe	379.1	203.3	46.38
	Ca	3979.7	2444.4	38.58

[1] By difference. [2] By ICP-OES analysis.

2.2. Pyrolysis System and Experimental Procedure

The slow pyrolysis system is shown in Figure 1. A gas supply, gas flowmeter, tubular resistance furnace (OTF-1200X, Hefei, China), condensation unit, filter unit, and N-containing gas collection unit were all included in the system. At the start of each experiment, a 5.00 ± 0.02 g sample was mounted in the center of the furnace tube (constant temperature zone length: 150 mm) in a quartz boat (length: 80 mm). The system was purged for 40 min (400 mL/min) with high purity Ar (99.999%). Subsequently, the flow rate was adjusted to 200 mL/min, and the reactor was heated to the desired temperature (350 °C, 450 °C, 550 °C, or 650 °C) with a heating rate of 10 °C/min and then kept steady for 30 min to ensure the completion of pyrolysis. The outlet of the tubular quartz reactor was connected with the condensing device placed in the ice-water mixture. After that, the pyrolysis gas was filtered by absorbent cotton and entered the nitrogen-containing gas collection bottle containing 200 mL absorbent solution. The two kinds of NO_x precursors, NH_3 and

HCN, were absorbed by 5 g/L HBO_3 and 8 g/L NaOH solutions, respectively [29], and converted to the corresponding ions ($NH_3 \rightarrow NH_4^+$, HCN $\rightarrow CN^-$). To prevent interference, NH_3 and HCN collection experiments were carried out separately. Each experiment was duplicated under the same condition and the average value was adopted.

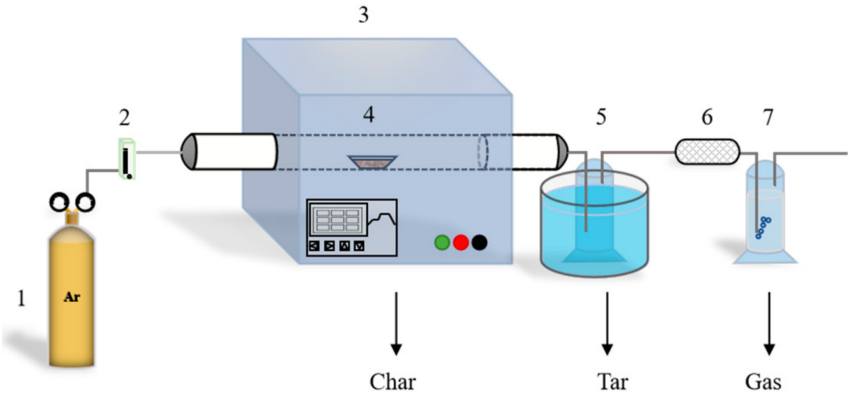

Figure 1. Schematic diagram of pyrolysis system: 1-gas supply, 2-gas flowmeter, 3-horizontal tubular resistance furnace, 4-quartz boat with samples, 5-condensation unit, 6-filter unit, 7-N-containing gas collection unit.

2.3. TG Analysis

The TG analysis of raw and acid-leached maize straw was performed by a thermal gravimetric analyzer (TGA 2, Mettler-Toledo, Greifensee, Switzerland) in the Ar atmosphere (50 mL/min). In each experiment, 5.00 ± 0.05 mg of the straw sample was heated from 30 °C to 900 °C at a constant heating rate of 10 °C/min. The experiments were performed twice to test the repeatability.

2.4. XPS Analysis

The nitrogen functional groups in the biomass and corresponding biochar were characterized using XPS analysis. The sample was uniformly glued to the conductive adhesive tape and degassed for 12 h. An X-ray photoelectron spectrometer (ESCALAB 250Xi, Thermo Fisher Scientific, Waltham, MA, USA) with a monochromatic Al K_α X-ray source (150 W, hv = 1486.6 eV) was used, the following were the operating conditions: a spot size of 650 µm, a voltage of 14.8 kV, a current of 1.6 A, a constant analyzer pass energy mode (100 eV for survey scans and 20 eV for narrow scans) and a pressure less than 10^{-10} mbar. The XPS results were evaluated by Thermo Avantage software. The Shirley-type background was subtracted and all spectra were calibrated based on the principal C1s peak at 285.0 eV [30–33]. Thereafter, the N1s signal was curve-resolved using peaks with a 70% Gaussian and 30% Lorentzian line shape and the FWHM of 1.4 eV [32]. Peaks at 398.8 ± 0.2 eV, 399.9 ± 0.2 eV, 400.4 ± 0.2 eV, 401.4 ± 0.2 eV and 402–405 eV corresponding to the energy positions were considered as N functional groups of pyridine-N (N-6), amine-N/amide-N/protein-N (N-A), pyrrole-N (N-5), quaternary-N/inorganic-N (N-Q/N-IN) and N-oxide (N-X), respectively [12,34–36].

2.5. Scanning Electron Microscopy (SEM)

The sample powers were fixed on the conductive adhesive tape and coated with a gold film. The morphology images of two biomass and corresponding char products were performed using an SEM device (SU3500, HITACHI, Tokyo, Japan, an accelerating voltage of 10 kV).

2.6. Calculations

The difference between the initial and final weight of containers was used to calculate char and tar production. According to the forms of pyrolysis product, nitrogen

compounds were classified into char-N, gas-N (NH_3-N, HCN-N) and rest-N (tar-N and other N-containing products). The following equations were used to measure the yields of char-N and nitrogen functional groups (group-N) in char products [36]:

$$Y_{char\text{-}N} = \frac{m_{char} \times w_{char\text{-}N}}{m_{biomass} \times w_N} \times 100\% \quad (1)$$

$$Y_{group\text{-}N} = \frac{A_{group\text{-}N}}{\sum A_{group\text{-}N}} \times Y_{char\text{-}N} \quad (2)$$

where $Y_{char\text{-}N}$ and $Y_{group\text{-}N}$ mean the yields of char-N and group-N in char products, respectively (wt%), $m_{biomass}$ and m_{char} mean the mass of biomass and corresponded char products, respectively (g), w_N and $w_{char\text{-}N}$ mean the N contents from biomass and char products, respectively (wt%), and $A_{group\text{-}N}$ means the peak area of each nitrogen functional group in char according to the XPS analysis.

Based on relevant Chinese standards, the absorption solutions of NO_x gaseous precursors were analyzed using a UV2800 ultraviolet spectrophotometer (UNICO, Princeton, NJ, USA) [37,38]. Yields of these gas-N were calculated by Equation (3):

$$Y_{gas\text{-}N} = \frac{c_n \times \mathrm{V}}{m_{biomass} \times w_N} \times 100\% \quad (3)$$

where $Y_{gas\text{-}N}$ means the yields of NH_3-N or HCN-N (wt%), c_n is the concentrations of NH_3-N or HCN-N in the absorption solutions (g/mL), and V represents the volume of absorption solution (200 mL).

3. Results and Discussion

3.1. Characteristics of Raw/Acid Leached Maize Straw

TG and derivative thermogravimetric (DTG) curves of RMA and AMS samples are shown in Figure 2. Similarly, both two biomass samples were found in three stages of mass loss. According to relevant researches, these three stages were summarized as water evaporation (below 200 °C), rapid decomposition of hemicellulose and cellulose (around 200–400 °C), and slow pyrolysis of lignin and other residual materials (above 400 °C) [39–41]. By comparison with the TG curve of RMS (Figure 2a), the second pyrolysis stage of AMS began later (at around 300 °C). This hysteresis was due to the fact that AAEMs in the ash could promote the decomposition of cellulose and hemicellulose under low temperature [42]. A shoulder peak at 305.67 °C was observed during the pyrolysis of acid-leached maize straw (Figure 2a). It is understood that the peak at around 300 °C originated from hemicellulose degradation [43]. RMS had a maximum degradation rate of 8.43%/min at 322.33 °C, which was lower than AMS's (10.60%/min at 356.83 °C) (Figure 2b). As the temperature increased to about 350 °C, the AMS samples continued to release volatiles at a rapid rate, while the weightlessness rate of RMS slowed. These results are consistent with those reported in other studies [42,44,45]. According to the description of Zareihassangheshlaghi et al. [23], the increased concentration of metal impurities on the surface of straw biomass ash could be found during the conversion, which could promote the formation of agglomeration and char, thereby hindering the following biomass decomposition. Also, acid-leaching treatment could increase the porosity of biomass and promote the conversion of cellulose and hemicellulose into sugars, leading to a large release of volatiles [20].

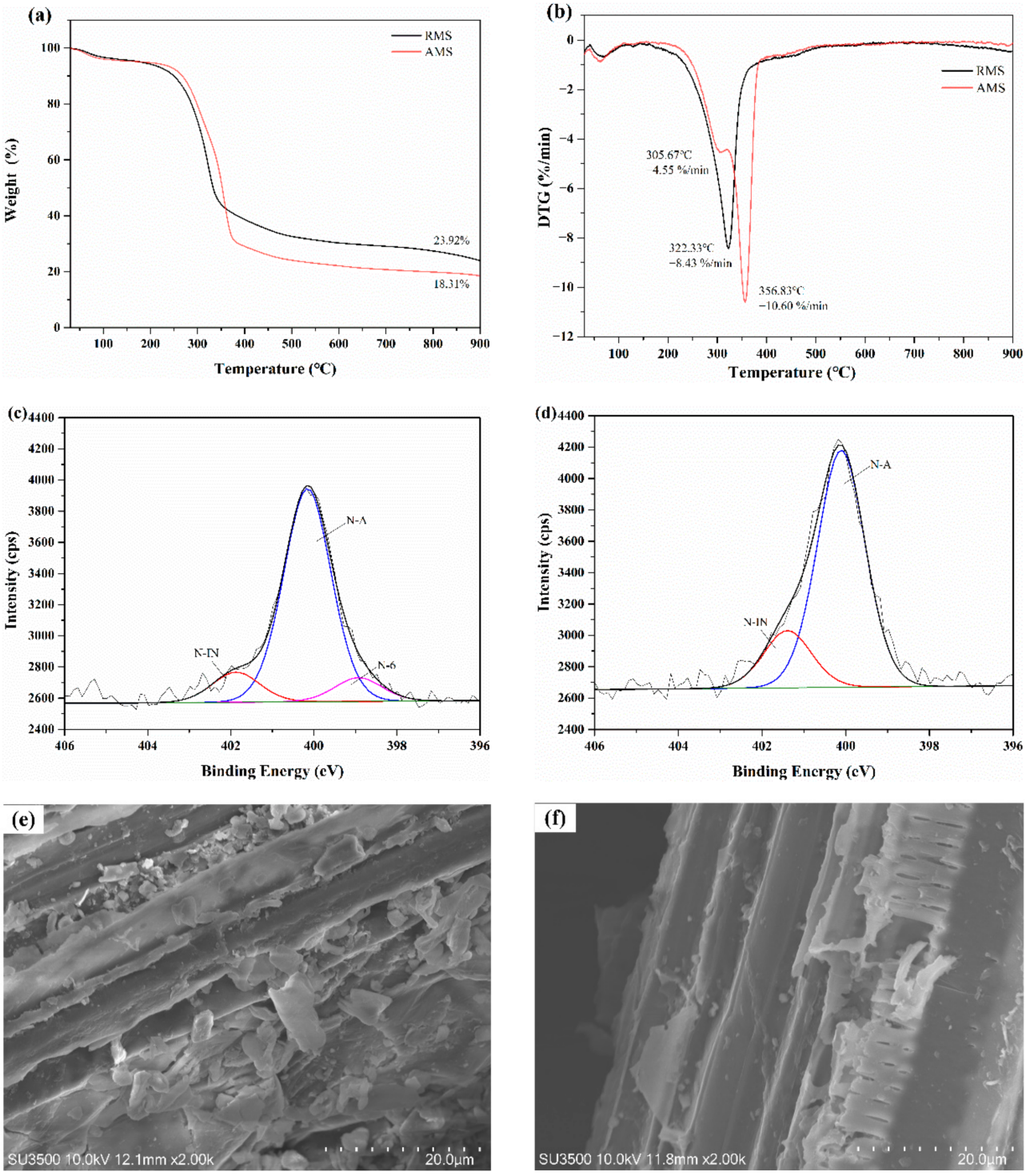

Figure 2. Curves of TG, DTG, and XPS analysis and SEM images of raw/acid leached maize straw: (**a**) TG curves; (**b**) DTG curves; (**c**) XPS analysis of raw maize straw (RMS); (**d**) XPS analysis of acid-leached maize straw (AMS); (**e**) SEM image of RMS; (**f**) SEM image of AMS.

The functional group characteristics of specific elements in different samples were investigated using XPS analysis. The predominant peak was observed in both biomass samples at 399.9 ± 0.2 eV, which can be verified as N-A (Figure 2c,d) [12]. Maize can absorb nitrogen elements from soil and chemical fertilizer for growth, the fixed nitrogen in biomass mainly existing in the forms of amine-N/amide-N/protein-N [46]. Some nitrogen in biomass exists in inorganic nitrogen such as NH_4^+-N, while quaternary-N groups are

usually observed after heating treatment [47–49], thus the small peaks at 401.88 eV of RMS and 401.39 eV of AMS should be defined as N-IN in this study (Figure 2c,d) [36]. Moreover, the RMS spectrum contained the N-6 peak at 398.93 eV, which was missing in the AMS spectrum. These losses may be due to the high solubility of pyridine nitrogen and its reaction with acids during the pre-treatment. Moreover, a lot of floccules and small particles were observed in raw maize straw compared to acid leached straw (Figure 2e,f), which mainly belong to various salty, inorganic constituents in ash.

3.2. Distribution of Pyrolysis Products

In this study, solid products were represented by biochar, liquid products consisted of tar and condensed water, and the remaining non-condensable gases were referred to as gaseous products. According to the TG analysis reported above, the moisture in biomass was extracted before 200 °C, so the change of liquid products from 350 °C to 650 °C could be attributed to different tar productions. Under different temperatures, similar change trends in the pyrolysis product yields were obtained for the two biomass samples (Figure 3). Biochar was the predominant product during biomass samples pyrolysis at 350 °C, accounting for 48.55% for RMS and 44.81% for AMS. When the temperature increased to 450 °C, the char proportions decreased quickly for RMS (39.06%) and AMS (35.66%) due to the devolatilization. Gaseous product yields increased as the temperature increased from 350 °C to 450 °C, while liquid product yields increased from 450 °C to 550 °C and peaked at 550 °C. The highest yields of liquid products were 42.33% and 46.92% for RMS and AMS, respectively. During pyrolysis at low temperatures, the unstable chemical bonds of biomass break quickly and primarily produce non-condensable gases, while the ring cracking reactions in lignin and char were much stronger at higher temperatures and a large amount of tar are generated [50]. More surface folds and structural cracking were observed in SEM images from high-temperature pyrolysis (Figure 4). As the reaction temperature increased from 550 °C to 650 °C, the liquid product yields fell rapidly, which were attributed to the secondary decomposition of tar products. Moreover, higher solid product yields and lower liquid product yields were observed in RMS groups than that in AMS groups at the same pyrolysis temperature. According to Figure 4, ash agglomeration and sintering of particles resulted in larger ash particles coating the surface of char products from RMS. The acid-leaching pre-treatment could increase the porosity of the biomass and promoted the removal of volatiles [20].

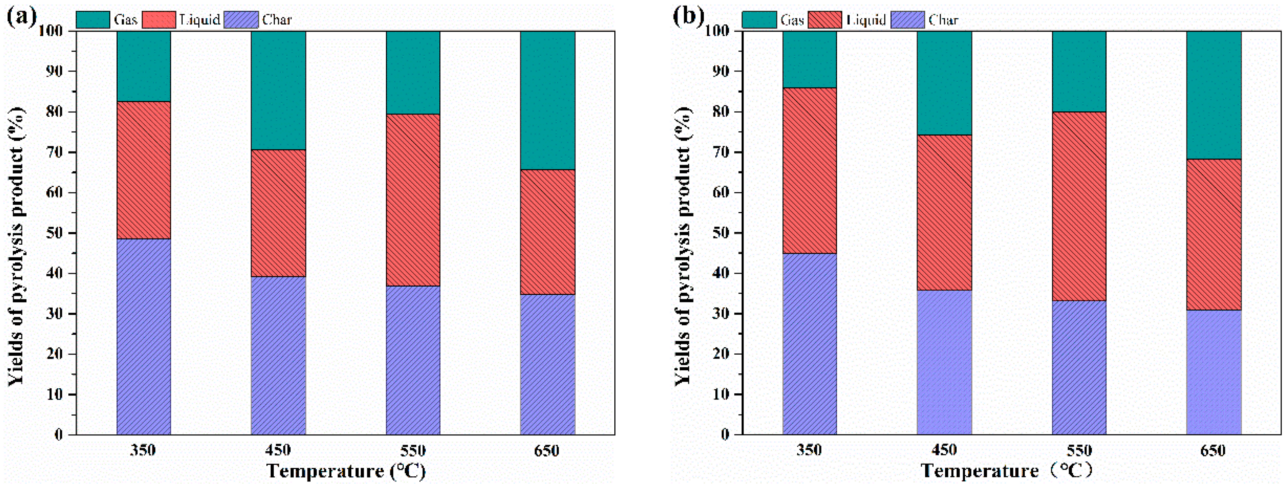

Figure 3. Pyrolysis products from RMS (**a**) and AMS (**b**) under different pyrolysis temperatures.

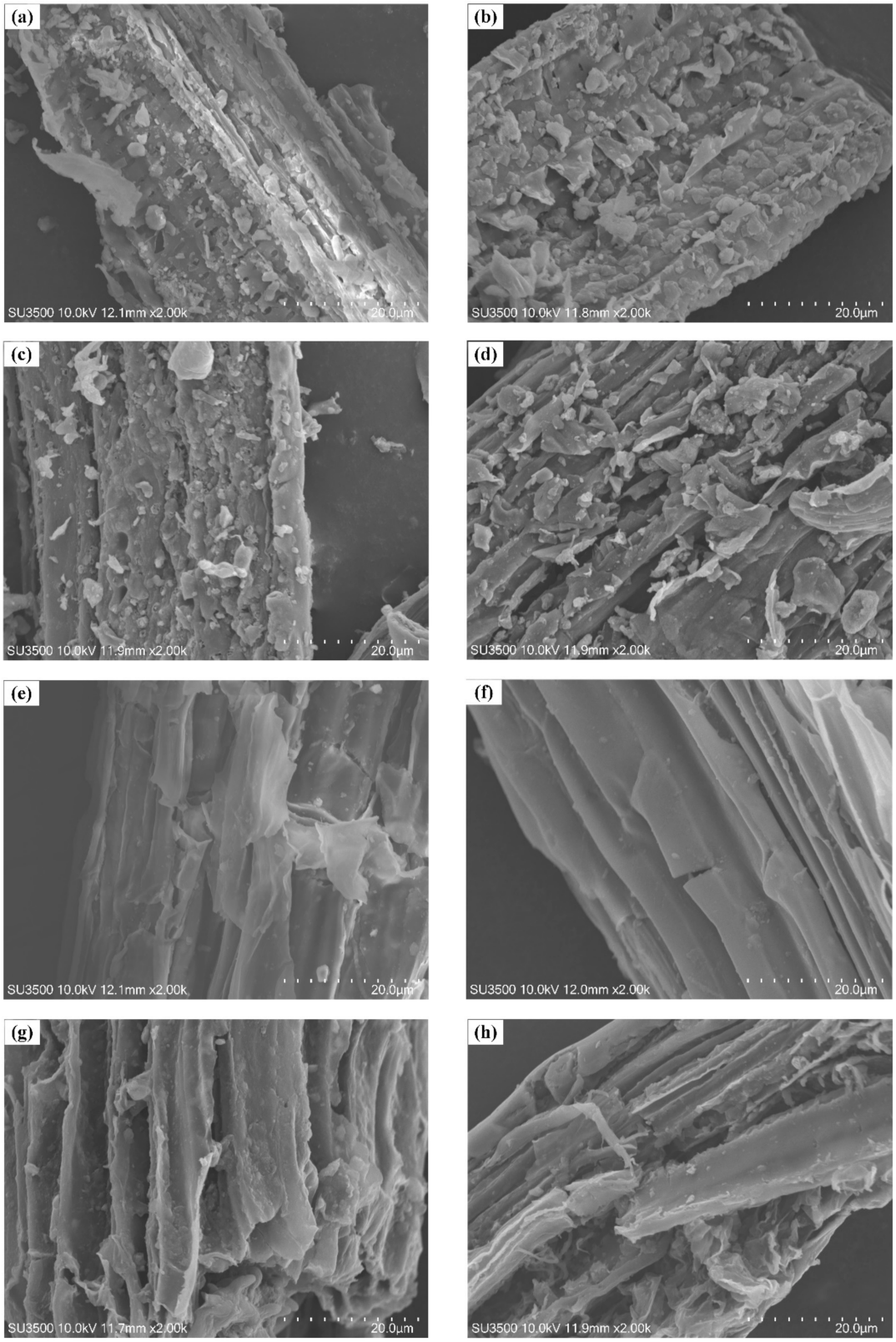

Figure 4. SEM images of the char products: (**a**) RMS_{350}; (**b**) RMS_{450}; (**c**) RMS_{550}; (**d**) RMS_{650}; (**e**) AMS_{350}; (**f**) AMS_{450}; (**g**) AMS_{550}; (**h**) AMS_{650}.

3.3. Distribution of Gaseous NO_x Precursors

As shown in Figure 5, NH_3 was the dominant NO_x gaseous precursors during pyrolysis of the two straw samples. According to the literature, when the fuel-N mostly existed as aromatic ring-N, the dominant gaseous NO_x precursors was HCN. When it existed in amine-N groups, NH_3 would become the key intermediate product. The rapid increase of NH_3 yield from 350 °C to 450 °C was primarily due to the decomposition of N-A, while the decomposition of char and tar could also produce NH_3 at the higher temperature. For HCN-N yield, it remained at a low level in the low-temperature pyrolysis for RMS and AMS, while a large increase was achieved at 650 °C. This meant that more heterocyclic-N was broken and HCN was released as the temperature rose.

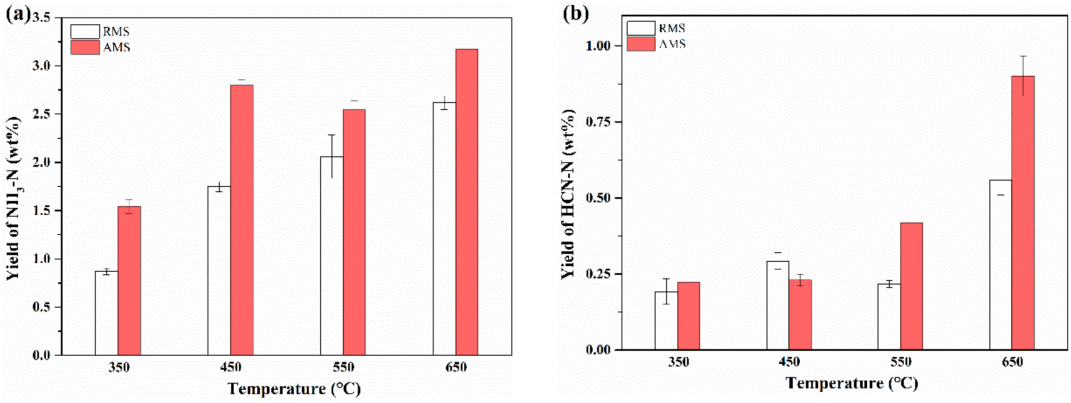

Figure 5. Yields of NH_3-N (**a**) and HCN-N (**b**) from RMS and AMS under different pyrolysis temperatures.

In the literature, it is reported that the removal of AAEM species from coal fuel before pyrolysis will reduce nitrogen conversion to NO_x gaseous precursors, but the situation is more complicated for biomass fuels [51]. Different amino acid structures have different nitrogen release characteristics during the chemical chain cracking. Potassium, for example, has been found to promote the NH_3-N production during aspartic acid pyrolysis, while inhibiting the HCN-N conversion from phenylalanine thermal decomposition [6]. By comparison with RMS, AMS released more NH_3-N at each pyrolysis experiment, while obtained much higher HCN-N yields in high-temperature pyrolysis. The highest NH_3-N and HCN-N yields were 3.17% ± 0.14% and 0.90% ± 0.07%, respectively, obtained from AMS pyrolysis at 650 °C. It's clear that the gas-N proportion was small for the total fuel-N. In the following part, we investigated the characteristics of char-N at various temperatures to further quantitatively confirm the nitrogen conversion from the two biomass samples pyrolysis.

3.4. Nitrogen Migration in Char-N during Biomass Pyrolysis

During pyrolysis, C, H, O, N, and S elements can be removed in various compound forms. However, since decarburization and denitrification take far longer than other reactions like dehydrogenation and deoxygenation, the increased carbon and nitrogen contents could be observed in biochar compared to the biomass sample (Table 2).

Table 2. Ultimate analysis (wt%, dry basis) of char products from raw/acid-leached maize straw.

Sample	C	H	S	O [1]	N
RMS_{350}	53.47 ± 0.19	3.71 ± 0.03	0.18 ± 0.03	40.70 ± 0.28	1.94 ± 0.04
RMS_{450}	54.56 ± 0.06	3.16 ± 0.04	0.29 ± 0.03	40.18 ± 0.18	1.82 ± 0.04
RMS_{550}	56.32 ± 0.16	2.45 ± 0.05	0.35 ± 0.04	39.19 ± 0.30	1.69 ± 0.04
RMS_{650}	57.92 ± 0.16	1.75 ± 0.03	0.29 ± 0.04	38.63 ± 0.28	1.41 ± 0.04

Table 2. *Cont.*

Sample	C	H	S	O [1]	N
AMS_{350}	58.56 ± 0.16	4.40 ± 0.03	0.65 ± 0.06	34.49 ± 0.29	1.91 ± 0.04
AMS_{450}	61.42 ± 0.14	3.87 ± 0.04	0.93 ± 0.04	31.78 ± 0.27	2.01 ± 0.04
AMS_{550}	63.93 ± 0.20	2.98 ± 0.08	0.64 ± 0.06	30.37 ± 0.38	2.09 ± 0.04
AMS_{650}	65.52 ± 0.20	2.36 ± 0.04	0.53 ± 0.05	29.83 ± 0.35	1.77 ± 0.06

[1] By difference.

The XPS spectra of biochar obtained at different pyrolysis temperatures are shown in Figure 6 and yields of nitrogen functional groups in the solid phase are shown in Figure 7. The biochar obtained from low-temperature pyrolysis kept some residual N-A groups and N-IN groups, which eventually vanish at 450 °C and higher temperatures. They were considered as the main source of NH_3-N in low-temperature pyrolysis [49]. N-6 and N-5 were mainly produced from N-A through direct cyclization, dimerization, and other reactions [52,53]. During the pyrolysis process, N-5 and N-6 dominated in nitrogen functional groups from solid products and accounted for more than 50% of biochar-N. The yields of N-6 and N-5 increased with the temperature in the range from 350 °C to 450 °C, but decreased at higher temperatures due to the secondary decomposition (Figure 7). The ring-opening reaction of N-5 was the important way of HCN formation [54]. The binding energies of N-IN and N-Q groups were very close (401.4 ± 0.2 eV). Considering the thermal stability, N-IN could easily decompose when heated, while N-Q was primarily formed by the cyclo-condensation and hydrogenation reaction of N-6 at high temperature [55]. Previous studies have reported that N-6 and N-Q conversions play an important role in NH_3-N generation at high pyrolysis temperature [36,56]. N-X stands for various nitrogen oxide functional groups, which can be observed in char products under each temperature. Zhan et al. [29] suggested that it could be produced by the combination of N-6 and oxygen functional groups.

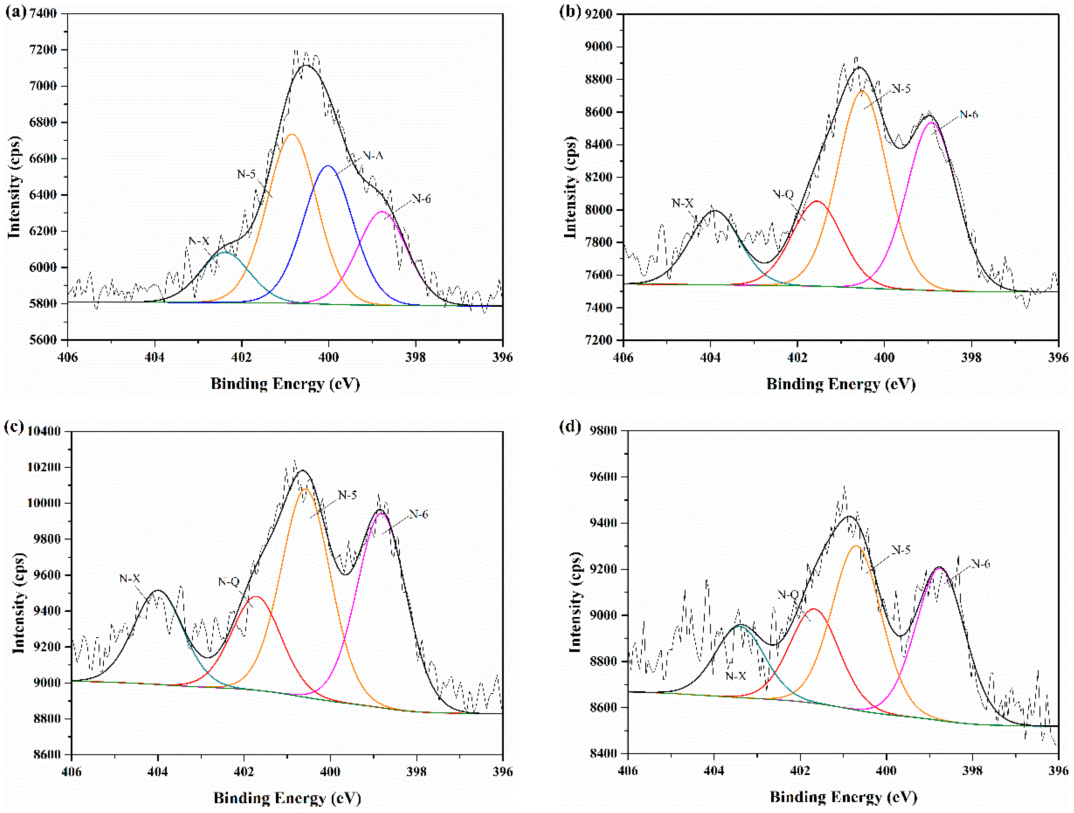

Figure 6. *Cont.*

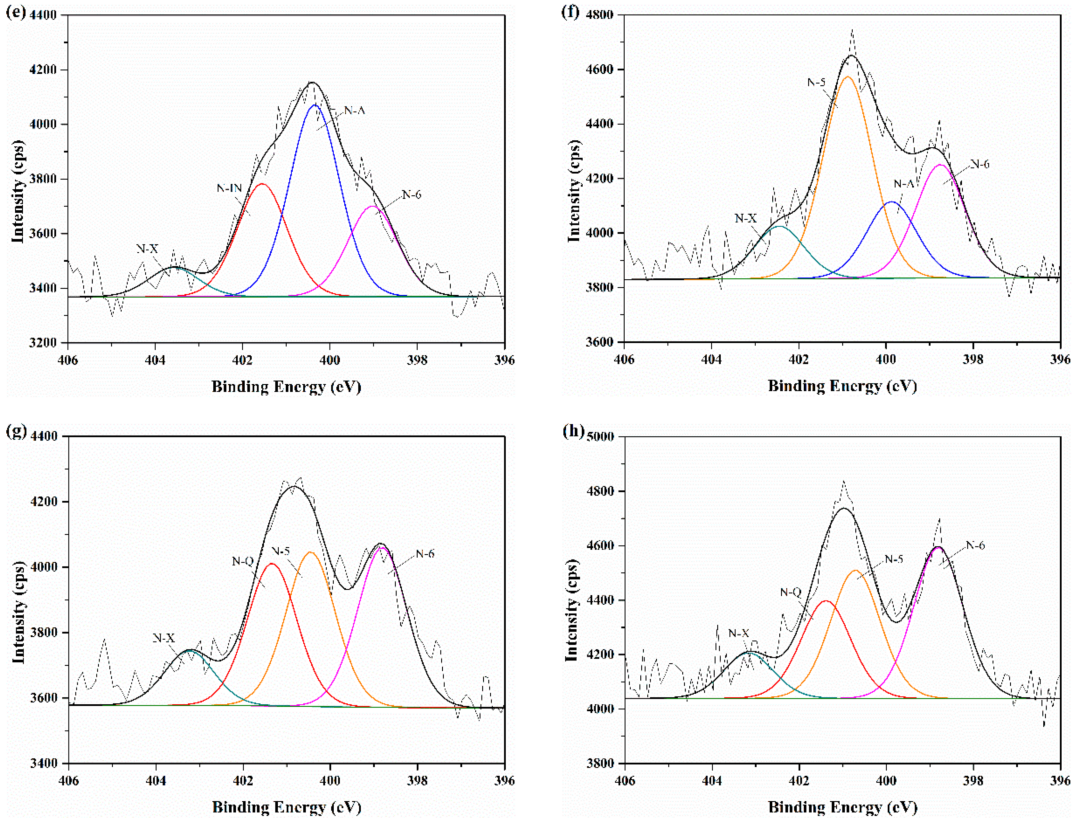

Figure 6. XPS analyses of the char products at various temperatures: (**a**) RMS_{350}; (**b**) RMS_{450}; (**c**) RMS_{550}; (**d**) RMS_{650}; (**e**) AMS_{350}; (**f**) AMS_{450}; (**g**) AMS_{550}; (**h**) AMS_{650}.

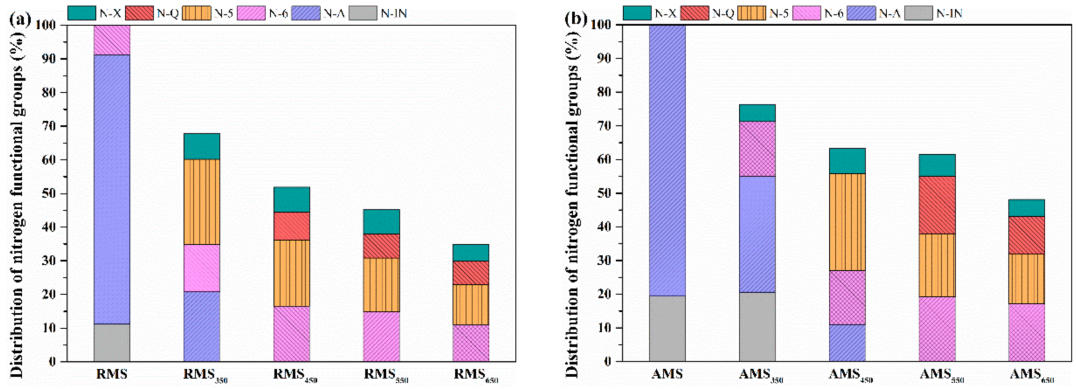

Figure 7. Yields of nitrogen functional groups in char products from RMS (**a**) and AMS (**b**) under different pyrolysis temperatures.

For nitrogen conversion in RMS pyrolysis, N-A yield dramatically dropped from 80.00 wt% to 20.82 wt% at 350 °C, while the corresponding gaseous-N (NH_3-N and HCN-N) only accounted for 1.06 wt%. It meant that in addition to the conversion of N-A to gaseous-N and N-5 and N-6 in char-N, a large part of N-A flowed into tar products. Moreover, by comparing the pyrolysis performance of RMA and AMS, delayed removals of N-IN and N-A were found in AMS pyrolysis with the same temperature. As the temperature increased from 350 °C to 450 °C, N-IN was totally converted, and N-A yield showed a decrease from 34.57 wt% to 10.94 wt%, which were responsible for the significant increase in NH_3-N yields in AMS pyrolysis (Figure 5a).

Based on the characteristic analysis of the pyrolysis products and related literature [12,36,57], nitrogen migration pathways during raw and acid-leached maize straw

pyrolysis were illustrated in Figure 8. Thermal decomposition of N-A and N-IN was the main source of NH_3-N at low temperature, and the conversions of N-5 (char-N) and heterocyclic-N (tar-N) contributed to HCN-N yield at high temperature.

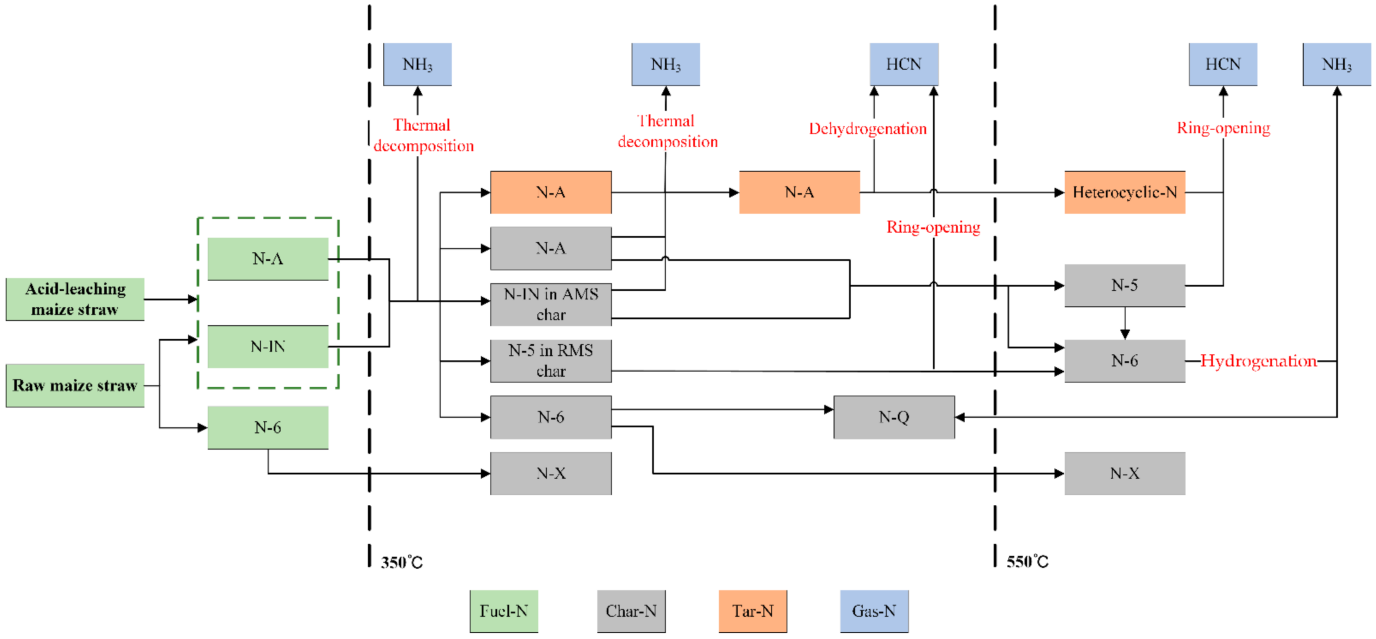

Figure 8. Possible fuel-N migration pathways during pyrolysis of RMA and AMS.

3.5. Nitrogen Distribution in Pyrolysis Products of Raw and Acid-Leached Maize Straw

In general, the distribution of nitrogen in each phase product from RMS and AMS were shown in Table 3. The yield of rest-N was detected by difference, of which tar-N accounted for more than 90%. During low temperature (350 °C, 450 °C) pyrolysis processes, more than half of the biomass-N was deposited in biochar products. As pyrolysis temperature increased, it can be seen that nitrogen elements gradually flowed from solid products to gas and tar. Among the three-phase products, gas-N took a small part of the total, and the majority of nitrogen was combined in the tar products during high-temperature pyrolysis. The proportion of gaseous NO_x precursors of sludge and some industrial waste biomass can be higher than that of straw biomass [49]. Zhan et al. [49] reported the gas-N yield (<8.5 wt%) and variation trend from straw biomass pyrolysis between 200 °C and 500 °C, which was close to the results in this study.

Table 3. Nitrogen distribution (wt%) in different pyrolysis products from RMS and AMS.

Sample	Char-N	Gas-N	Tar-N and Others [1]
RMS_{350}	67.80	1.06	31.14
RMS_{450}	51.87	2.04	46.09
RMS_{550}	45.23	2.28	52.49
RMS_{650}	34.98	3.18	61.84
AMS_{350}	76.39	1.76	21.85
AMS_{450}	63.32	3.03	33.65
AMS_{550}	61.53	2.96	35.51
AMS_{650}	48.13	4.07	47.80

[1] By difference.

The higher tar-N yield was obtained from RMS than AMS with the same temperature, AAEMs in the ash may promote the generation of tar-N in raw straw. N-rich tar products can be used in the production of high value-added chemicals, which is meaningful for

industrial production. However, the complex nitrogen bonds in tar were labile and would cause severe NO_x emissions during fuel combustion. The slow nitrogen release from a stable char structure would support nitrogen control of straw fuel combustion. Although a slight increase of gas-N yield was found in AMS, the char-N yield was much higher than that of RMS. The char-N yield (76.39 wt%) was peaked at 350 °C from AMS pyrolysis, which was higher than that of other studies [34,49,58]. These results can provide some guidance for straw fuel modification and its low NO_x combustion.

4. Conclusions

The pyrolysis performance and nitrogen migration pathways of raw and acid leached straw biomass at various temperatures were investigated in this paper. The acid-leaching pretreatment effectively reduced the AAEMs in the ash of the straw. Thermogravimetric analysis showed that AMS released more volatiles than RMS during pyrolysis, but the maximum degradation rate of the former moved to a higher temperature than that of the latter. NH_3 dominated in gaseous NO_x precursor from slow pyrolysis of two straw biomass. The conversions of unstable N-IN and N-A groups in straw contributed to the NH_3 generation at low pyrolysis temperatures (350 °C and 450 °C), while more than half of the HCN was formed from the secondary reactions of N-5 in char and other heterocyclic-N in tar products. Particularly, higher char-N and gas-N yields were observed from AMS than RMS with the same temperature. The highest char-N yield of 76.39 wt% was obtained from AMS pyrolysis at 350 °C. By operating low pyrolysis temperature and acid-leaching treatment, the fuel nitrogen can be effectively stored in the stable char-N structure, rather than gaseous NO_x precursors or labile tar-N, which could provide support for NO_x emissions control from straw fuel combustion.

Author Contributions: Conceptualization, H.L., H.M. and Y.Z.; software, N.Z., Y.Y.; methodology, Q.H.; writing—original draft preparation, H.L.; writing—review and editing, M.P. and H.B.D.; supervision, Y.Z. and R.D. All authors have read and agreed to the published version of the manuscript.

Funding: This study was supported by the National Natural Science Foundation of China (Grant No. U20A2086; Grant No. 51806242), the Special Project on Innovation Methodology, Ministry of Science and Technology of China (No. 2020IM020900), the Inner Mongolia Autonomous Region Science and Technology Plan Project (Grant No. 2020GG0123), the Yantai Educational-Local Synthetic Development Project (Grant No. 2019XDRHXMXK25, No. 2019XDRHXMQT36), and DBFZ Deutsches Biomasseforschungszentrum Gemeinnützige GmbH.

Institutional Review Board Statement: Not applicable.

Informed Consent Statement: Informed consent was obtained from all subjects involved in the study.

Data Availability Statement: The data that supported the findings of this study are available from the corresponding author upon reasonable request.

Acknowledgments: We appreciate the support from the Key Laboratory of Clean Production and Utilization of Renewable Energy, Ministry of Agriculture and Rural Affairs, China; DBFZ Deutsches Biomasseforschungszentrum gemeinnützige GmbH, Department Thermo-chemical Conversion; National Center for International Research of BioEnergy Science and Technology, Ministry of Science and Technology, China; the National Energy R&D Center for Biomass, National Energy Administration of China; and Beijing Municipal Key Discipline of Biomass Engineering.

Conflicts of Interest: The authors declare no conflict of interest.

References

1. Zhou, Y.; Zhang, Z.; Zhang, Y.; Wang, Y.; Yu, Y.; Ji, F.; Ahmad, R.; Dong, R. A comprehensive review on densified solid biofuel industry in China. *Renew. Sustain. Energy Rev.* **2016**, *54*, 1412–1428. [CrossRef]
2. Houshfar, E.; Skreiberg, Ø.; Todorović, D.; Skreiberg, A.; Løvås, T.; Jovović, A.; Sørum, L. NO_x emission reduction by staged combustion in grate combustion of biomass fuels and fuel mixtures. *Fuel* **2012**, *98*, 29–40. [CrossRef]

3. EPA. Nitrogen Oxides (NOx), Why and How They Are Controlled. 1999. Available online: https://www3.epa.gov/ttncatc1/dir1/fnoxdoc.pdf (accessed on 26 March 2021).
4. He, F.; Li, Y.; Dou, S.; Yi, W. Design and Experiments on Residential Heating Furnace with Biomass Smoldering. *Nongye Jixie Xuebao/Trans. Chin. Soc. Agric. Mach.* **2006**, *37*, 75–78.
5. Susastriawan, A.A.P.; Badrawada, I.G.G.; Budi, D.P. An effect of primary air draft and flow rate on thermal perfor-mance and CO/CO_2 emission of the domestic stove fed with the briquette of coconut shell. *Biomass Convers. Biorefin.* **2020**, *10*, 1099–1104. [CrossRef]
6. Ren, Q.; Zhao, C. NO_x and N_2O precursors (NH_3 and HCN) from biomass pyrolysis: Interaction between amino acid and mineral matter. *Appl. Energy* **2013**, *112*, 170–174. [CrossRef]
7. Shah, I.A.; Gou, X.; Zhang, Q.; Wu, J.; Wang, E.; Liu, Y. Experimental study on NO_x emission characteristics of oxy-biomass combustion. *J. Clean. Prod.* **2018**, *199*, 400–410. [CrossRef]
8. Tian, F.; Li, B.; Chen, Y.; Li, C. Formation of NO_x precursors during the pyrolysis of coal and biomass. Part V. Pyrolysis of a sewage sludge. *Fuel* **2002**, *81*, 2203–2208. [CrossRef]
9. Ren, Q. NO_x and N_2O precursors from biomass pyrolysis. *J. Anal. Calorim.* **2014**, *115*, 881–885. [CrossRef]
10. Wang, Y.; Dong, B.; Fan, Y.; Hu, Y.; Zhai, X.; Deng, C.; Xu, Y.; Shen, D.; Dai, X. Nitrogen transformation during pyrolysis of oilfield sludge with high polymer content. *Chemosphere* **2019**, *219*, 383–389. [CrossRef] [PubMed]
11. Zaker, A.; Chen, Z.; Wang, X.; Zhang, Q. Microwave-assisted pyrolysis of sewage sludge: A review. *Fuel Process. Technol.* **2019**, *187*, 84–104. [CrossRef]
12. Tian, Y.; Zhang, J.; Zuo, W.; Chen, L.; Cui, Y.; Tan, T. Nitrogen conversion in relation to NH_3 and HCN during microwave pyrolysis of sewage sludge. *Environ. Sci. Technol.* **2013**, *47*, 3498–3505. [CrossRef]
13. Becidan, M.; Skreiberg, Ø.; Hustad, J.E. NO_x and N_2O precursors (NH_3 and HCN) in pyrolysis of biomass residues. *Energy Fuel* **2007**, *21*, 1173–1180. [CrossRef]
14. Hansson, K.; Samuelsson, J.; Tullin, C.; Åmand, L. Formation of HNCO, HCN, and NH_3 from the pyrolysis of bark and nitrogen-containing model compounds. *Combust. Flame* **2004**, *137*, 265–277. [CrossRef]
15. Cheng, L.; Ma, F.; Ranwala, D. Nitrogen storage and its interaction with carbohydrates of young apple trees in response to nitrogen supply. *Tree Physiol.* **2004**, *24*, 91–98. [CrossRef]
16. Ren, Q.; Zhao, C. Evolution of fuel-N in gas phase during biomass pyrolysis. *Renew. Sustain. Energy Rev.* **2015**, *50*, 408–418. [CrossRef]
17. Sher, F.; Pans, M.A.; Afilaka, D.T.; Sun, C.; Liu, H. Experimental investigation of woody and non-woody biomass combustion in a bubbling fluidised bed combustor focusing on gaseous emissions and temperature profiles. *Energy* **2017**, *141*, 2069–2080. [CrossRef]
18. Cheng, S.; Qiao, Y.; Huang, J.; Wang, W.; Wang, Z.; Yu, Y.; Xu, M. Effects of Ca and Na acetates on nitrogen transformation during sewage sludge pyrolysis. *Proc. Combust. Inst.* **2019**, *37*, 2715–2722. [CrossRef]
19. Ren, Q.; Zhao, C.; Wu, X.; Liang, C.; Chen, X.; Shen, J.; Tang, G.; Wang, Z. Effect of mineral matter on the formation of NO_x precursors during biomass pyrolysis. *J. Anal. Appl. Pyrol.* **2009**, *85*, 447–453. [CrossRef]
20. Dong, Q.; Zhang, S.; Zhang, L.; Ding, K.; Xiong, Y. Effects of four types of dilute acid washing on moso bamboo pyrolysis using Py–GC/MS. *Bioresour. Technol.* **2015**, *185*, 62–69. [CrossRef]
21. Long, J.; Song, H.; Jun, X.; Sheng, S.; Lun-shi, S.; Kai, X.; Yao, Y. Release characteristics of alkali and alkaline earth metallic species during biomass pyrolysis and steam gasification process. *Bioresour. Technol.* **2012**, *116*, 278–284. [CrossRef]
22. Wigley, T.; Yip, A.C.K.; Pang, S. Pretreating biomass via demineralisation and torrefaction to improve the quality of crude pyrolysis oil. *Energy* **2016**, *109*, 481–494. [CrossRef]
23. Zareihassangheshlaghi, A.; Beidaghy Dizaji, H.; Zeng, T.; Huth, P.; Ruf, T.; Denecke, R.; Enke, D. Behavior of metal impurities on surface and bulk of biogenic silica from rice husk combustion and the impact on ash-melting tendency. *ACS Sustain. Chem. Eng.* **2020**, *8*, 10369–10379. [CrossRef]
24. Oudenhoven, S.R.G.; Westerhof, R.J.M.; Kersten, S.R.A. Fast pyrolysis of organic acid leached wood, straw, hay and bagasse: Improved oil and sugar yields. *J. Anal. Appl. Pyrol.* **2015**, *116*, 253–262. [CrossRef]
25. AQSIQ. *Proximate Analysis of Solid Biofuels, GB/T 28731-2012*; General Administration of Quality Supervision, Inspection and Quarantine of the People's Republic of China: Beijing, China, 2012.
26. Zhao, N.; Li, B.; Chen, D.; Bahargul, T.; Wang, R.; Zhou, Y.; Annegarn, H.J.; Pemberton-Pigott, C.; Dong, R.; Ju, X. The effect of coal size on $PM_{2.5}$ and PM-bound polycyclic aromatic hydrocarbon (PAH) emissions from a domestic natural cross-draft stove. *J. Energy Inst.* **2019**, *93*, 542–551. [CrossRef]
27. Li, Q.; Zhao, Y.; Chen, H.; Hou, P.; Cheng, X. Effect of cornstalk ash on the microstructure of cement-based material under sulfate attack. IOP conference series. *Earth Environ. Sci.* **2019**, *358*, 52010.
28. Guo, J.; Cui, X.; Sun, H.; Zhao, Q.; Wen, X.; Pang, C.; Dong, R. Effect of glucose and cellulase addition on wet-storage of excessively wilted maize stover and biogas production. *Bioresour. Technol.* **2018**, *259*, 198–206. [CrossRef]
29. Zhan, H.; Yin, X.; Huang, Y.; Yuan, H.; Wu, C. NO_x precursors evolving during rapid pyrolysis of lignocellulosic industrial biomass wastes. *Fuel* **2017**, *207*, 438–448. [CrossRef]
30. Nefedov, V.I.; Salyn, Y.V.; Leonhardt, G.; Scheibe, R. A comparison of different spectrometers and charge corrections used in X-ray photoelectron spectroscopy. *J. Electron. Spectrosc.* **1977**, *10*, 121–124. [CrossRef]

31. Nesbitt, H.W.; Bancroft, G.M.; Tse, J.S.; Gao, X.; Skinner, W.; Zakaznova-Herzog, V.P. High-resolution valence-band XPS spectra of the nonconductors quartz and olivine. *Phys. Rev. B.* **2005**, *72*, 205113.
32. Sawyer, R.; Nesbitt, H.W.; Secco, R.A. High resolution X-ray Photoelectron Spectroscopy (XPS) study of K_2O–SiO_2 glasses: Evidence for three types of O and at least two types of Si. *J. Non Cryst. Solids* **2012**, *358*, 290–302. [CrossRef]
33. Stoch, J.; Ladecka, M. An XPS study of the KCl surface oxidation in oxygen glow discharge. *Appl. Surf. Sci.* **1988**, *31*, 426–436. [CrossRef]
34. Gao, P.; Guo, D.; Liang, C.; Liu, G.; Yang, S. Nitrogen conversion during the rapid pyrolysis of raw/torrefied wheat straw. *Fuel* **2020**, *259*, 116227. [CrossRef]
35. Wei, L.; Wen, L.; Yang, T.; Zhang, N. Nitrogen transformation during sewage sludge pyrolysis. *Energy Fuel* **2015**, *29*, 5088–5094. [CrossRef]
36. Zhan, H.; Zhuang, X.; Song, Y.; Yin, X.; Wu, C. Insights into the evolution of fuel-N to NO_x precursors during pyrolysis of N-rich nonlignocellulosic biomass. *Appl. Energy* **2018**, *219*, 20–33. [CrossRef]
37. MOEP. *Water Quality-Determination of Cyanide Volumetric and Spectrophotometry, HJ 484-2009*; Ministry of Environmental Protection of the People's Republic of China: Beijing, China, 2009.
38. MOEP. *Water Quality-Determination of Ammonia Nitrogen-Nessler's Reagent Spectrophotometry, HJ 535-2009*; Ministry of Environmental Protection of the People's Republic of China: Beijing, China, 2009.
39. Deng, S.; Wang, X.; Tan, H.; Mikulčić, H.; Yang, F.; Li, Z.; Duić, N. Thermogravimetric study on the co-combustion characteristics of oily sludge with plant biomass. *Thermochim. Acta* **2016**, *633*, 69–76. [CrossRef]
40. Huang, J.; Liu, J.; Chen, J.; Xie, W.; Kuo, J.; Lu, X.; Chang, K.; Wen, S.; Sun, G.; Cai, H.; et al. Combustion behaviors of spent mushroom substrate using TG-MS and TG-FTIR: Thermal conversion, kinetic, thermodynamic and emission analyses. *Bioresour. Technol.* **2018**, *266*, 389–397. [CrossRef] [PubMed]
41. Wang, T.; Peng, L.; Ai, Y.; Zhang, R.; Lu, Q. Pyrolytic behaviors of decocting residues of *Rhodiola rosea*. *J. Anal. Appl. Pyrol.* **2018**, *129*, 61–65. [CrossRef]
42. Eom, I.; Kim, K.; Kim, J.; Lee, S.; Yeo, H.; Choi, I.; Choi, J. Characterization of primary thermal degradation features of lignocellulosic biomass after removal of inorganic metals by diverse solvents. *Bioresour. Technol.* **2011**, *102*, 3437–3444. [CrossRef]
43. Zhang, S.; Zhang, H.; Su, Y.; Xu, D.; Zhu, S.; Liu, X. Effects of torrefaction and organic-acid leaching pretreatment on the pyrolysis behavior of rice husk. *Energy* **2018**, *149*, 804–813. [CrossRef]
44. Meng, A.; Zhou, H.; Qin, L.; Zhang, Y.; Li, Q. Quantitative and kinetic TG-FTIR investigation on three kinds of biomass pyrolysis. *J. Anal. Appl. Pyrol.* **2013**, *104*, 28–37. [CrossRef]
45. Yang, C.; Lu, X.; Lin, W.; Yang, X.; Yao, J. TG-FTIR Study on Corn Straw Pyrolysis-influence of Minerals. *Chem. Res. Chin. Univ.* **2006**, *22*, 524–532. [CrossRef]
46. Yuan, S.; Tan, Z.; Huang, Q. Migration and transformation mechanism of nitrogen in the biomass-biochar-plant transport process. *Renew. Sustain. Energy Rev.* **2018**, *85*, 1–13. [CrossRef]
47. Ma, D.; Zhang, G.; Areeprasert, C.; Li, C.; Shen, Y.; Yoshikawa, K.; Xu, G. Characterization of NO emission in combustion of hydrothermally treated antibiotic mycelial residue. *Chem. Eng. J.* **2016**, *284*, 708–715. [CrossRef]
48. Yuan, S.; Zhou, Z.; Li, J.; Wang, F. Nitrogen conversion during rapid pyrolysis of coal and petroleum coke in a high-frequency furnace. *Appl. Energy* **2012**, *92*, 854–859. [CrossRef]
49. Zhan, H.; Zhuang, X.; Song, Y.; Huang, Y.; Liu, H.; Yin, X.; Wu, C. Evolution of nitrogen functionalities in relation to NO precursors during low-temperature pyrolysis of biowastes. *Fuel* **2018**, *218*, 325–334. [CrossRef]
50. Wang, T.; Dong, X.; Jin, Z.; Su, W.; Ye, X.; Dong, C.; Lu, Q. Pyrolytic characteristics of sweet potato vine. *Bioresour. Technol.* **2015**, *192*, 799–801. [CrossRef]
51. Chang, L.; Zhao, Y.; Xie, K. Effect of inherent minerals on the release of fuel-nitrogen during coal pyrolysis. *Energy Sources* **2005**, *27*, 1019–1027. [CrossRef]
52. Choi, S.; Ko, J. Analysis of cyclic pyrolysis products formed from amino acid monomer. *J. Chromatogr. A* **2011**, *1218*, 8443–8455. [CrossRef]
53. Zhan, H.; Zhuang, X.; Song, Y.; Yin, X.; Cao, J.; Shen, Z.; Wu, C. Step pyrolysis of N-rich industrial biowastes: Regulatory mechanism of NO precursor formation via exploring decisive reaction pathways. *Chem. Eng. J.* **2018**, *344*, 320–331. [CrossRef]
54. Zhang, J.; Tian, Y.; Cui, Y.; Zuo, W.; Tan, T. Key intermediates in nitrogen transformation during microwave pyrolysis of sewage sludge: A protein model compound study. *Bioresour. Technol.* **2013**, *132*, 57–63. [CrossRef]
55. Li, C.; Tan, L.L. Formation of NO_x and SO_x precursors during the pyrolysis of coal and biomass. Part III. Further discussion on the formation of HCN and NH_3 during pyrolysis. *Fuel* **2000**, *79*, 1899–1906. [CrossRef]
56. Kambara, S.; Takarada, T.; Yamamoto, Y.; Kato, K. Relation between functional forms of coal nitrogen and formation of nitrogen oxide (NO_x) precursors during rapid pyrolysis. *Energy Fuel* **1993**, *7*, 1013–1020. [CrossRef]
57. Liu, H.; Yi, L.; Hu, H.; Xu, K.; Zhang, Q.; Lu, G.; Yao, H. Emission control of NO_x precursors during sewage sludge pyrolysis using an integrated pretreatment of Fenton peroxidation and CaO conditioning. *Fuel* **2017**, *195*, 208–216. [CrossRef]
58. Li, Y.; Hong, C.; Wang, Y.; Xing, Y.; Chang, X.; Zheng, Z.; Li, Z.; Zhao, X. Nitrogen migration mechanism during pyrolysis of penicillin fermentation residue based on product characteristics and quantum chemical analysis. *ACS Sustain. Chem. Eng.* **2020**, *8*, 7721–7740. [CrossRef]